Title

Comparing Experimental Measurements of Limiting Current in Polymer Electrolytes with Theoretical Predictions

Journal

Journal of The Electrochemical Society, 166(14)

ISSN

0013-4651

Authors

Gribble, Daniel A
Frenck, Louise
Shah, Deep B
et al.

Publication Date

2019

DOI

10.1149/2.0391914jes

Peer reviewed

Comparing Experimental Measurements of Limiting Current in Polymer Electrolytes with Theoretical Predictions

Daniel A. Gribble[a], Louise Frenck[a,b], Deep B. Shah[a,b], Jacqueline A. Maslyn[a,b], Whitney S. Loo[a], Katrina Irene S. Mongcopa[a], Danielle M. Pesko[a], Nitash P. Balsara[a,b,c,d,*]

[a] Department of Chemical and Biomolecular Engineering, University of California, Berkeley, California 94720, USA

[b] Materials Sciences Division, Lawrence Berkeley National Laboratory, Berkeley, California 94720, USA

[c] Joint Center for Energy Storage Research (JCESR), Lawrence Berkeley National Laboratory, Berkeley, California 94720, USA

[d] Energy Storage and Distributed Resources Division, Lawrence Berkeley National Laboratory, Berkeley, California 94720, USA

Corresponding Author:

* Nitash P. Balsara: E-mail: nbalsara@berkeley.edu, Address: Department of Chemical Engineering, 201 Gilman Hall, University of California, Berkeley, CA 94720-201462, USA,

Phone: (+1) 510-642-8973.

Notes:

The authors declare no competing financial interest.

Abstract

The limiting current is an important transport property of an electrolyte as it provides an upper bound on how fast a cell can be charged or discharged. We have measured the limiting current in lithium-lithium symmetric cells with a standard polymer electrolyte, a mixture of poly(ethylene oxide) and lithium bis(trifluoromethane) sulfonamide salt at 90 °C. The cells were polarized with increasing current density. The steady-state cell potential was a smooth function of current density until the limiting current was exceeded. An abrupt increase in cell potential was taken as an experimental signature of the limiting current. The electrolyte mixture was fully characterized using electrochemical methods to determine the conductivity, salt diffusion coefficient, cation transference number, and thermodynamic factor as a function of salt concentration. We used Newman's concentrated solution theory to predict both cell potential and salt concentration profiles as functions of position in the cell at the experimentally applied current density. The theoretical limiting current was taken to be the current at which the calculated salt concentration at the cathode was zero. We see quantitative agreement between experimental measurements and theoretical predictions for the limiting current. This agreement is obtained without resorting to any adjustable parameters.

Keywords

limiting current, concentrated solution theory, polymer electrolytes, ion transport

1. Introduction

Great efforts are being made to develop new electrolyte replacements for rechargeable lithium batteries.[1–8] Traditional electrolytes used in lithium batteries are mixtures of salts dissolved in cyclic carbonates. The limited stability of these electrolytes at the operating potential of the batteries affects both cycle life and safety.[9–15] There is thus considerable interest in developing new electrolytes that overcome these limitations.[1,3,6,8,16–18] One approach is to replace the solvent by a polymer. When a battery is not being used, the salt concentration is uniform throughout the electrolyte phase. The passage of a current through the battery results in salt concentration gradients due to the mobility of both the cation and anion. The magnitudes of these gradients increase with increasing current until the limiting current is reached. Limiting current is defined as the current at which the salt concentration at the cathode equals zero.[19–23] There are relatively few publications on the measurement of limiting current in lithium battery electrolytes, and they are all limited to liquid electrolytes.[24–26] In this study we present measurements of limiting current in a well-studied polymer electrolyte: a mixture of poly(ethylene oxide) (PEO) and lithium bis(trifluoromethane) sulfonamide (LiTFSI) salt.

We use Newman's concentrated solution theory to model ion transport in our electrolytes. Ion transport in both liquid and polymeric electrolytes depends on four concentration-dependent transport parameters: ionic

conductivity (□), salt diffusion coefficient (D), transference number of the cation with respect to the solvent (t_{+}^{0}), and the thermodynamic factor $(1+d\ln\gamma_{\pm}/d\ln m)$, where $\gamma_{\pm}$ is the mean molal activity coefficient of the salt and m is the molality of the electrolyte.[23] These parameters were measured independently, and used to predict the dependence of limiting current in a Li|PEO/LiTFSI|Li symmetric cell on salt concentration.[27] We thus compare experimentally measured limiting current values with theoretical predictions without resorting to any adjustable parameters.

2. Experimental

2.1 Electrolyte Preparation

The PEO (Polymer Source) used in this study has a molecular weight of 935 kg mol^{-1} and dispersity of 1.14. All steps were conducted in an argon-filled glovebox. Both the PEO and LiTFSI (Sigma Aldrich) were dried in the glovebox antechamber under vacuum at 90 °C and 130 °C for 1 and 3 days, respectively. Electrolytes were prepared by dissolving PEO and LiTFSI in anhydrous tetrahydrofuran (Sigma Aldrich) and stirring at 60 °C until completely dissolved. The amount of salt was varied such that the r_{av} value, the average molar ratio of lithium ions to ether oxygens in the polymer, ranged from values of 0.01 to 0.31, with 15 samples prepared in total. The solvated electrolytes were then subsequently dried on a hotplate at 60 °C, and then placed in the glovebox antechamber under vacuum for 24 hours at 90 °C.

2.2 Cell Preparation

The lithium metal foil (MTI Corp) used as electrodes has a purity of 99.97%. All samples and cells were prepared inside an argon-filled glovebox with water and oxygen levels below 0.5 and 1 ppm, respectively. The lithium electrodes were prepared by brushing lithium foil and pressing it with a mechanical press to create a clean, smooth surface. The lithium foil was backed with a nickel foil for mechanical support and even current distribution. The total thickness (approximately 300 μm) of both electrodes is measured prior to assembly. Li|PEO/LiTFSI|Li symmetric cells were prepared by melting the polymer electrolyte at 90 °C on a hotplate into a 250 μm thick silicone spacer with an inner diameter of 0.3175 cm and sandwiching the electrolyte with the lithium electrodes. To ensure that the spacer did not preclude contact between the electrolyte and the electrodes, the cells were overfilled to thicknesses as large as 300 μm. After assembling the lithium/polymer/lithium symmetric cell the total thickness was measured and the thickness of the electrolyte was determine by subtracting the thickness of the lithium foils. Nickel tabs were placed on the nickel side of both electrodes, and the whole cell was vacuum sealed in laminated pouch material, as electrochemical experiments were performed outside the glovebox.

We prepared cells containing electrolytes with a nominal thickness of 250 μm and salt concentrations of r_{av} = 0.02, 0.05, 0.065, and 0.085. Cells were annealed at 90 °C in a custom heating stage for 4 hours prior to electrochemical characterization. Electrochemical experiments were

performed at 90 °C using a Biologic VMP3 potentiostat paired with EC Lab software. Lithium symmetric cells were preconditioned before experimentation using five polarization cycles with an applied current density (i) of 0.02 mA cm^{-2} for 4 hour in each direction, with a 2 hour open circuit relaxation step between each polarization step. The purpose of preconditioning the cell is to stabilize the solid electrolyte interface (SEI) that forms between the electrolyte and lithium metal. This was confirmed by performing electrochemical impedance spectroscopy (EIS) with a frequency range of 1 MHz to 100 mHz and amplitude of 60 mV. Time independent EIS data were taken as a signature of a stable SEI.

2.3 Limiting Current Experiments

During experiments to determine the limiting current, current density through the cells was increased in a stepwise manner from i = 0.02 to 1.50 mA cm^{-2}. All experiments were conducted at 90 °C. A polarization cycle for one current density experiment consisted of polarization in one direction until the potential reached steady-state and then a two hour open circuit step to allow for relaxation, followed by polarization in the opposite direction and then the same open circuit rest step. The time required to reach steady-state varied from approximately 1 hour for low salt concentrations (r_{av} = 0.02) to 2 hours for higher salt concentrations (r_{av} = 0.085). In most cases, cells were used for one or two current density cycles as the low mechanical rigidity of PEO leaves it vulnerable to the nucleation and growth of lithium

dendrites.[28,29] Polarization time was minimized to reduce the influence of dendritic growth on our measurements. EIS experiments were performed before and after each polarization step to determine the bulk and interfacial impedances. Both positive and negative steady-state potentials (Φ_{SS}) for each polarization cycle were recorded. After experimentation, cells were disassembled in the glovebox and cell thickness was measured. This value was used to determine the electrolyte thickness (L) used in calculations after subtracting the thickness of the electrodes.

3. Results and Discussion

Figure 1 shows the time-dependence of cell potential, Φ (solid blue line, left axis), and the applied current density, i (dashed red line, right axis), of two cells with salt concentration r_{av} = 0.02. In Figure 1a, the cell was first polarized at a low current density, i = 0.04 mA cm^{-2}. The cell potential increases with increasing time and reaches a plateau at time t = 1 h. The applied current density was then changed to zero and results in relaxation of the cell potential. Qualitatively similar results are obtained when the cell is polarized with i = -0.04 mA cm^{-2} (Figure 1a). It should be noted that the measured open circuit potential is slightly different from zero (Figure 1a) due to unavoidable temperature gradients in the cell and the Seebeck effect.[30]

In Figure 1b, we show results obtained when the cell with r_{av} = 0.02 was polarized at a high current density, i = 0.42 mA cm^{-2}. In this case, the cell potential first increases slowly with time. At t = 0.32 h, the cell potential, Φ, shoots up. We take this to be an indication that the limiting current (i_L) has been exceeded. As the salt concentration at the cathode approaches zero, transport limitations prevent the formation of a stable concentration profile; as a result, Φ is unbounded.[23]

The experiments described in the previous paragraph were repeated for several values of r_{av} and i, and the results are summarized in Figure 2, where we plot $\Delta\Phi_f$ /L, the potential obtained at the end of the polarization

step, as a function of iL, the current density used for that polarization step. We chose these two parameters to normalize our results for variations in electrolyte thicknesses. The value of $\Delta\Phi_f$ is obtained after contributions from the interfacial impedance are subtracted according to Ohm's law, as reported in Ref 27. Before commencing the polarization step, complex impedance was acquired for a frequency range of 1 MHz to 100 mHz at an amplitude of 60 mV. The data were analyzed in the form of a Nyquist plot and fit to an equivalent electrical circuit suitable for a symmetric cell with nonblocking electrodes to obtain R_i, the interfacial resistance of the cell, as described in previous publications.[32] The value of R_i thus obtained, was used to calculate $\Delta\Phi_f$ ($\Delta\Phi_f = \Delta\Phi_{f,measured} - iR_iA$, where $\Delta\Phi_{f,measured}$ is the measured potential drop and A is the cell area). In low current density experiments, the potential reaches a plateau that we refer to as $\Delta\Phi_{SS,Expt}$. This is taken to be the potential at the end of the polarization step. To correct for the Seebeck effect, the reported values of Φ_{SS} are averages for the positive and negative applied current densities. For a given salt concentration, the magnitude of $\Delta\Phi_{SS,Expt}$ increases more-or-less linearly with i. In this regime, $\Delta\Phi_f$ and $\Delta\Phi_{SS,Expt}$ are identical. For example, for the case $r_{av} = 0.05$, a linear dependence of $\Delta\Phi_{SS,Expt}$ versus iL is seen up to $iL = 0.0175$ mA cm^{-1}. When the normalized current density is increased to 0.0181 mA cm^{-1}, Φ does not approach a plateau and $\Delta\Phi_f$ increases abruptly (Figure 2). At this current density $\Delta\Phi_{SS,Expt}$ is undefined. We thus only report $\Delta\Phi_f$ for such cases. The potentials $\Delta\Phi_f$ and $\Delta\Phi_{SS,Expt}$ are experimentally measured with corrections for interfacial

impedance. We call $\Delta\Phi_{SS,Expt}$ the potential measured experimentally at steady state for current density below the limiting current density (i.e. stabilized potential), while $\Delta\Phi_f$ is the final potential recorded at current densities above the limiting current density (i.e. when the potential diverges). We define the limiting current density, i_L, as the average of the highest current densities for which $\Delta\Phi_{SS,Expt}$ was observed and the current density at which Φ_{SS} was not observed. Half of the difference between these two current densities is taken as the error. The data in Figure 2 thus enable quantifying the relationship between i_L and r_{av}. Due to the frequency of cell failures, we were unable to obtain reliable data above a salt concentration of $r_{av} = 0.085$.

We use Newman's concentrated solution theory[23] to predict the limiting current in our electrolytes (iL) using the methodology described by Pesko et. al.[27] The first step is to fully characterize the electrolyte, i.e., measure the ionic conductivity (κ), the salt diffusion coefficient (D), the ideal transference number ($t_{+,ideal}$), and the thermodynamic factor $-(1+d\ln\gamma_{\pm}/d\ln m)$, where $\gamma_{\pm}$ is the mean molal activity coefficient of the salt and m is molality, as a function of salt concentration. Our approach for measuring these parameters is described in Refs 31 and 32. The ionic conductivity is measured using ac impedance, the salt diffusion coefficient is measured by restricted diffusion, the ideal transference number is measured by the steady state current method pioneered by Bruce and Vincent and data for concentration cells is combined with the ideal transference number measurements to obtain the thermodynamic factor.[31,32] Previous work by Pesko et al. suggests non-

idealities for PEO/LiTFSI mixtures are not strongly dependent upon molecular weight above 5 kg mol^{-1}.[31] The experiment to determine $(1+d\ln\gamma_{\pm}/d\ln m)$ is very resource intensive; in this paper we utilized the average of previously reported values (Ref 31) of $dU/d\ln m$, where U is the open-circuit potential of PEO/LiTFSI concentration cells, for PEO with molecular weights of 5 and 175 kg mol^{-1}, anticipating that the values for our 35 kg mol^{-1} system will fall somewhere in between. The thermodynamic factor is then calculated according to Equation 8 in Ref 31. In Figure 3 we present κ, D, and $t_{+,ideal}$ as a function of r_{av} (Some data for κ has been previously reported).[33] The parameter $t_{+,ideal}$ is measured using the approach proposed by Bruce and Vincent.[34,35] This approach gives the cation transference number for thermodynamically ideal electrolytes at infinite dilution. Also included Figure 3 is salt concentration, c, in units of mol cm^{-3}, as a function of r_{av}. The approach to determining c is given in Refs 31 and 32. Experimental data in Figure 3 were fit to polynomial expressions (shown on their respective plots) to reduce the influence of experimental noise on our analysis.

An important electrolyte characteristic is the transference number. The relationship between the rigorously defined transference number, $t_{+¿^0¿}$, and $t_{+,ideal}$ was quantified in Ref 36 and is given by Equations 1 and 2:

$$t_{+,ideal}=\frac{1}{1+Ne}, \quad \textbf{(1)}$$

$$Ne=2¿), \quad \textbf{(2)}$$

where T is temperature, R is the gas constant (8.314 J mol^{-1} K^{-1}), F is Faraday's constant (96,485 C mol^{-1}), and Ne is a dimensionless parameter we call the Newman number.[32,36,37] The cation and anion transference numbers are related such that $t_{-,0}$ = 1 - $t_{+,0}$. Fitted parameters from Figure 3 are used to calculate (1+dlnγ±/dln$m$), the resulting plot is shown in Figure 3e.

Since the concentration dependence of κ, D, and $1+\frac{dln\gamma_{\pm}}{dlnm}$ are known (Figures 3 a, b and e), measurements of $t_{+,ideal}$ can be used to determine $t_{-,0}$ (or equivalent $t_{+,0}$) using equations 1 and 2, the resulting plot is presented Figure 3f. Large discrepancies between $t_{+,0}$ and $t_{+,\mathrm{ideal}}$ are seen at all salt concentrations (Figures 3c and 3f). Unlike $t_{+,\mathrm{ideal}}$, values for $t_{+,0}$ are not bound between zero and one. In this case we witness the occurrence of negative transference numbers at several salt concentrations. Negative transference numbers have been previously reported for similar PEO electrolytes,[31,32,38,39] indicating the formation of charged clusters and correlated motion of unlike charges. The microscopic origin of negative transference numbers in these systems has not yet been elucidated.

For a given value of fixed applied current density, i, the spatial dependence of salt concentration in the cell, $r(x)$, is given by Equation 3:

$$\int_{r(x=0)}^{r(x)} \frac{D(r)c(r)}{r\,t_{-,0}(r)}\,dr = \frac{-iL}{F}\left(\frac{x}{L}\right) \quad \textbf{(3)}$$

Note that all the relevant concentration dependent properties of the electrolyte are grouped on the left side of Equation 3. Our objective is to determine $r(x)$ for a given value of r_{av} and i. This is done by first guessing $r(x = 0)$ and solving for $r(x)$ using Equation 1 for all x from 0^+ to L by numerical integration. This enables determination of a calculated value of r_{av}, and if it does not agree with the specified value of r_{av}, then $r(x = 0)$ is changed until convergence.

Once $r(x)$ is known, then the spatially-dependent steady-state potential, $\Phi_{SS}(x)$, is calculated using Equation 4:

$$\Phi_{SS}(x) = F \int_{r(x=L)}^{r(x)} \frac{D(r)c(r)}{r\, t_{+,ideal}(r)\kappa(r)t_{-,0}(r)} dr \quad \textbf{(4)}$$

where we have assumed that $\Phi ss = 0$ at $x = 0$. Equation 4 applies to the electric potential in the bulk electrolyte phase. Since potential is only measured at $x = L$, it is important to subtract the potential drop due to interfacial impedance from the measured potential before comparisons between experiment and theory are made, as is the case in the present study.

The collection of transport properties and their corresponding polynomial fits relevant for calculation of $r(x)$ and $\Phi ss(x)$ are plotted as a function of salt concentration in Figure 4. Polynomial fits to these concentration-dependent transport parameters are shown in Equations 5 and 6.

The fitted equation to the data in Figure 4a used to compute the right side of Equation 3 is

$$\frac{D(r)c(r)}{r\,t_{-¿^0(r)}} = ar^5 + br^4 + cr^3 + dr^2 + er + f ¿ \quad \textbf{(5)}$$

with a = 1.088E-4, b = -9.889E-5, c = 3.280E-5, d = -4.750E-6, e = 2.670E-7, and f = -9.425E-10.

The fitted equation to the data in Figure 4b used to compute the right side of Equation 4 is

$$\frac{D(r)c(r)}{r\,t_{+,ideal}(r)\kappa(r)t_{-¿^0(r)}} = a'r^4 + b'r^3 + c'r^2 + d'r + e¿' + f' \quad \textbf{(6)}$$

with a' = 6.638E-2, b' = -5.455E-2, c' = 1.678E-2, d' = -2.081E-3, e' = 2.400E-5, and f' = 2.238E-5.

In Figure 5, we plot Φss and r as functions of x/L, for r_{av} = 0.085. These results were obtained by combining Equations 3 through 6. Equation 5 is used to numerically integrate the left side of Equation 3. Equation 6 is used to numerically integrate the right side of Equation 4. When the applied current is zero, there are no salt concentration gradients (dashed line in Figure 5b). At low current density (i = 0.389 mA cm^{-2}), Φ_{SS} and r are approximately linear functions of x. Non-linearities are evident with increasing current density. At i_{SS} = 1.56 mA cm^{-2}, $r(x/L = 1)$ is zero. We define the current at which this happens to be the theoretically predicted limiting

current, i_L. Theoretical predictions for Φ_{SS} are limited to current densities less than i_L. Calculations of the type shown in Figure 4 were repeated for all salt concentrations studied (Supplementary Material: Section S1). The value of $r(x/L = 0)$ never exceeded 0.20, thus the integration of data presented in Figure 3 are limited to $0 \leq r \leq 0.20$. The upper bound of the range of relevant r values is shown by the vertical dashed lines in Figure 3.

The theoretically predicted potential drop across the electrode, $\Delta\Phi_{SS,Th}$, is equal to Φ_{SS} at $x/L = 0$. The solid curve in Figure 6 represents $\Delta\Phi_{SS,Th}/L$, the normalized potential drop, as a function of normalized current density iL for $r_{av} = 0.085$ (Figure 6a), where both axes are normalized by cell thickness. The terminus of this curve, represented by an 'x', represents the theoretical prediction for the limiting current. The circles in Figure 6 represent experimentally determined $\Delta\Phi_{SS,Exp}/L$ values for $r = 0.085$ (Figure 2). The dashed line in Figure 6 represents the experimentally determined limiting current density and is in quantitative agreement with the theoretical prediction. Below the limiting current we find reasonable agreement between the experimentally and theoretically determined normalized potential drops. It is important to note that the theoretical predictions are based entirely on transport properties that were measured independently. Similar plots to Figure 6 are shown in the Supplementary Material (Section S2) for electrolytes with $r_{av} = 0.02$, 0.05, and 0.065.

In the discussion above we have used concentrated solution theory to predict cell behavior and limiting current. A much simpler approach for estimating limiting current, based on dilute solution theory and the assumption that the salt diffusion coefficient and the cation transference number do not depend on salt concentration, leads to the following expression for the limiting current (Equation 7). We have also taken the liberty of using $t_{+,\text{ideal}}$ as the appropriate transference number.[40]

$$i_L = \frac{2C_b FD}{(1-t_{+,ideal})L} \qquad \textbf{(7)}$$

We now return to our experimental results and compare them with theoretical predictions. The experimentally measured limiting current as a function of salt concentration is shown in Figure 7 as triangles, where we plot the product $i_L L$ versus r_{av}. The predictions from concentrated solution theory are shown by solid red lines. The limiting current was determined theoretically using Equations 3 through 6 at the four salt concentrations where experiments were conducted, and the results are joined by straight red lines. The predictions from dilute solution theory are shown by dashed blue lines. In this case, the limiting current was calculated using Equation 7 at the four salt concentrations using experimentally determined values of c, D, and $t_{+,\text{ideal}}$ (Figure 3) at the value of r_{av} of interest, and the results were joined by straight lines. Note that all three parameters change significantly with salt concentration and thus our “dilute approximation” is based on data obtained by applying concentrated solution theory to experimental data

(Figure 3). Reasonable agreement between both of the theories and experiment is evident in Figure 7. For all practical purposes, and over the range of parameters considered in this work, the results of the rigorous approach based on numerical integration (Equations 3 through 6) are similar to those obtained using the relatively simple equation (Equation 7). Both models predict that i_L increases with increasing r_{av}, as seen in the experiments.

4. Conclusion

The limiting current in symmetric Li|PEO/LiTFSI|Li cells at 90 °C was determined experimentally as a function of average salt concentration in the

electrolyte. The time-dependence of the cell potential was recorded at fixed current densities. The steady-state cell potential was a smooth function of current density until a threshold; this threshold was taken as an indication that the applied current exceeded the limiting current. In separate experiments, the PEO/LiTFSI mixture was fully characterized using electrochemical methods to determine the ionic conductivity, salt diffusion coefficient, cation transference number, and the thermodynamic factor as a function of average salt concentration. All parameters are strong functions of salt concentration. This enabled calculation of cell potential and salt concentration profiles as a function of applied current density using Newman's concentrated solution theory.[23] The theoretical limiting current was taken to be the current at which the salt concentration at the cathode was found to be zero. We see quantitative agreement between experimental measurements and theoretical predictions. These models can be extended to different electrolyte chemistries to predict battery performance.[41]

Acknowledgements

This work was supported by the Assistant Secretary for Energy Efficiency and Renewable Energy, Office of Vehicle Technologies of the U.S. Department of Energy under Contract DE-AC02-05CH11231 under the Battery Materials Research Program.

425

426References

4271. M. Tatsumisago, F. Mizuno, and A. Hayashi, *J. Power Sources*, **159**, 193–
428199 (2006).

4292. J. L. Schaefer, D. A. Yanga, and L. A. Archer, *Chem. Mater.*, **25**, 834–839
430(2013).

4313. R. Khurana, J. L. Schaefer, L. A. Archer, and G. W. Coates, *J. Am. Chem.*
432*Soc.*, **136**, 7395–7402 (2014).

4334. A. Manuel Stephan, *Eur. Polym. J.*, **42**, 21–42 (2006)
434https://linkinghub.elsevier.com/retrieve/pii/S0014305705003733.

4355. A. Ulvestad, (2018) http://arxiv.org/abs/1803.04317.

4366. G. M. Veith et al., *ACS Energy Lett.*, **2**, 2084–2088 (2017).

4377. W. Zhou et al., *J. Am. Chem. Soc.*, **138**, 9385–9388 (2016).

4388. R. Bouchet et al., *Nat. Mater.*, **12**, 1–6 (2013)
439http://dx.doi.org/10.1038/namt3602.

4409. G. Gachot et al., *J. Power Sources*, **178**, 409–421 (2008).

44110. P. Arora, *J. Electrochem. Soc.*, **145**, 3647 (1998)
442http://jes.ecsdl.org/cgi/doi/10.1149/1.1838857.

44311. S. E. Sloop, J. B. Kerr, and K. Kinoshita, *J. Power Sources*, **119**–**121**, 330–
444337 (2003).

44512. Y. S. Yun, J. H. Kim, S.-Y. Lee, E.-G. Shim, and D.-W. Kim, *J. Power*
446*Sources*, **104**, 260–264 (2002)
447http://linkinghub.elsevier.com/retrieve/pii/S0378775301009600.

44813. E. P. Roth and C. J. Orendorff, *Interface Mag.*, **21**, 45–49 (2016).

44914. K. Xu, *Chem. Rev.*, **104**, 4303–4418 (2004).

45015. J. Wen, Y. Yu, and C. Chen, *Mater. Express*, **2**, 197–212 (2012)
451http://openurl.ingenta.com/content/xref?genre=article&issn=2158-
4525849&volume=2&issue=3&spage=197.

45316. W. Tang et al., *Energy Environ. Sci.*, **6**, 2093–2104 (2013).

45417. G. T. Kim et al., *J. Power Sources*, **196**, 2187–2194 (2011)

455http://dx.doi.org/10.1016/j.jpowsour.2010.09.080.

45618. K. Xu, S. Zhang, J. L. Allen, and T. R. Jow, *J. Electrochem. Soc.*, **149**, 457A1079 (2002).

45819. E. A. Hogge and M. B. Kraichman, *J. Am. Chem. Soc.*, **76**, 1431–1433 459(1954).

46020. J. Newman, *J. Electrochem. Soc.*, **113**, 1235 (2007).

46121. H. S. Sand, *Proc. Phys. Soc. London*, **17**, 496–534 (1899).

46222. B. Y. B. Levich, (1947).

46323. J. Newman and K. E. T. Alyea, *Electrochemical Systems*, Third., John Wiley 464& Sons, Inc., (2004).

46524. C. O. Laoire, E. Plichta, M. Hendrickson, S. Mukerjee, and K. M. Abraham, 466*Electrochim. Acta*, **54**, 6560–6564 (2009).

46725. J. W. Park, K. Yoshida, N. Tachikawa, K. Dokko, and M. Watanabe, *J.* 468*Power Sources*, **196**, 2264–2268 (2011) 469http://dx.doi.org/10.1016/j.jpowsour.2010.09.067.

47026. S. I. Lee et al., *Korean J. Chem. Eng.*, **19**, 638–644 (2002).

47127. D. M. Pesko et al., *J. Electrochem. Soc.*, **165**, A3186–A3194 (2018).

47228. K. J. Harry, thesis, University of California Berkeley (2006).

47329. C. Monroe and J. Newman, *J. Electrochem. Soc.*, **152**, A396 (2005) 474http://jes.ecsdl.org/cgi/doi/10.1149/1.1850854.

47530. H. Wang, U. Ail, R. Gabrielsson, M. Berggren, and X. Crispin, *Adv. Energy* 476*Mater.*, **5**, 1–6 (2015).

47731. D. M. Pesko, S. Sawhney, J. Newman, and N. P. Balsara, *J. Electrochem.* 478*Soc.*, **165**, A3014–A3021 (2018).

47932. D. M. Pesko et al., *J. Electrochem. Soc.*, **164**, E3569–E3575 (2017).

48033. K. I. S. Mongcopa et al., *ACS Macro Lett.*, **7**, 504–508 (2018).

48134. P. G. Bruce, M. T. Hardgrave, and C. A. Vincent, *J. Electroanal. Chem.* 482*Interfacial Electrochem.*, **271**, 27–34 (2002).

48335. J. Evans, C. A. Vincent, and P. G. Bruce, *Polymer (Guildf).*, **28**, 2324–2328 484(1987).

48536. N. P. Balsara and J. Newman, *J. Electrochem. Soc.*, **162**, A2720–A2722 486(2015).

48737. M. Doyle, *J. Electrochem. Soc.*, **142**, 3465 (2006).

48838. M. M. Doeff, P. Georén, J. Qiao, J. Kerr, and L. C. De Jonghe, **146**, 2024–4892028 (1999).

49039. A. Ferry, M. Doeff, and L. De Jonghe, *ECS*, **145**, 1586–1592 (1997).

49140. C. Monroe and J. Newman, *J. Electrochem. Soc.*, **150**, A1377 (2003).

49241. D. B. Shah et al., *Phys. Chem. Chem. Phys.*, **21**, 7857–7866 (2019).

493List of Symbols and Abbreviations

494

A	cell area (cm^2)
$(1+d\ln\gamma_{\pm}/d\ln m)$	thermodynamic factor
$t_{+,0}$	real cation transference number for non-ideal concentrated solutions
$t_{-,0}$	real anion transference number for non-ideal concentrated solutions
c	salt concentration (mol/cm^3)
D	salt diffusion coefficient (cm^2/s)
EIS	electrochemical impedance spectroscopy
F	Faraday constant (C/mol)
i	constant-valued applied current density (mA/cm^2)
i_L	limiting current density (mA/cm^2)
L	electrolyte thickness (μm)
LiTFSI	lithium bis(trifluoromethane) sulfonimide salt
m	molality (mol/kg)
Ne	Newman number
PEO	poly(ethylene oxide) polymer
r	molar concentration of lithium ions to ether oxygens ($r = [Li^+]/[EO]$)
R	gas constant (J/molK)
R_i	Interfacial resistance measured with impedance spectroscopy
$r(x)$	spatially dependent molar concentration of lithium ions to ether oxygens
r_{av}	average molar concentration of lithium ions to ether oxygens
SEI	solid electrolyte interface
T	temperature (K)
$t_{+,ideal}$	ideal cation transference number for infinitely dilute solutions
U	open circuit potential of a Li-PEO/LiTFSI-PEO/LiTFSI-Li concentration cell

x	cell coordinate defined such that $x = 0$ is at the anode and $x = L$ the cathode (μm)
$\gamma_{\pm}$	overall salt activity coefficient
$\Delta\Phi_{f}$	potential difference measured at the end of a polarization cycle without interfacial contribution (V)
$\Delta\Phi_{SS,Exp}$	experimentally determined potential drop across the electrodes above limiting current (V)
$\Delta\Phi_{f,measured}$	potential difference measured at the end of a polarization cycle (V)
$\Delta\Phi_{SS,Th}$	theoretically predicted potential drop across the electrodes (V)
κ	ionic conductivity (S/cm)
Φ	potential (mV)
Φ_{SS}	steady-state potential (mV)
$\Phi_{SS}(x)$	spatially dependent steady-state potential (mV)

495

496

497

498**Figures**

499

500

501

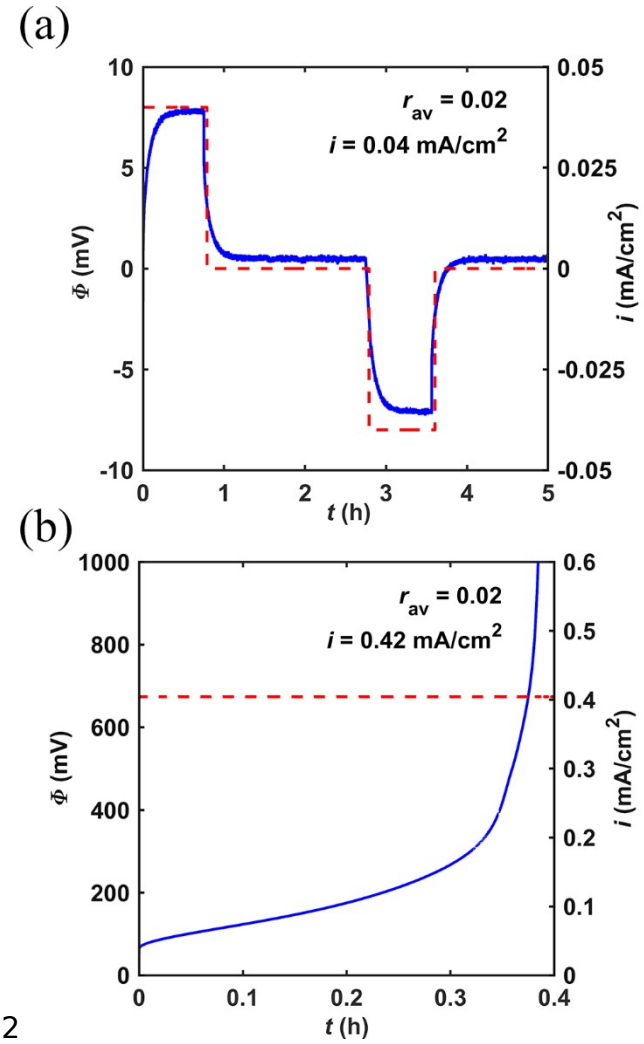

Figure 1: Cell potential, Φ (solid blue line, left axis), versus time, t, for two Li|PEO/LiTFSI|Li cells of salt concentration r_{av} = 0.02 at different magnitudes of applied current density, i (dashed red line, right axis). **(a)** Example of a cell reaching a steady-state potential during polarization at a low current density of i = 0.04 mA cm^{-2}; cell thickness L = 268 μm. **(b)** Example of potential diverging due to transport limitations above the limiting current density i_L during polarization at high current density i = 0.42 mA cm^{-2}; cell thickness L = 299 μm.

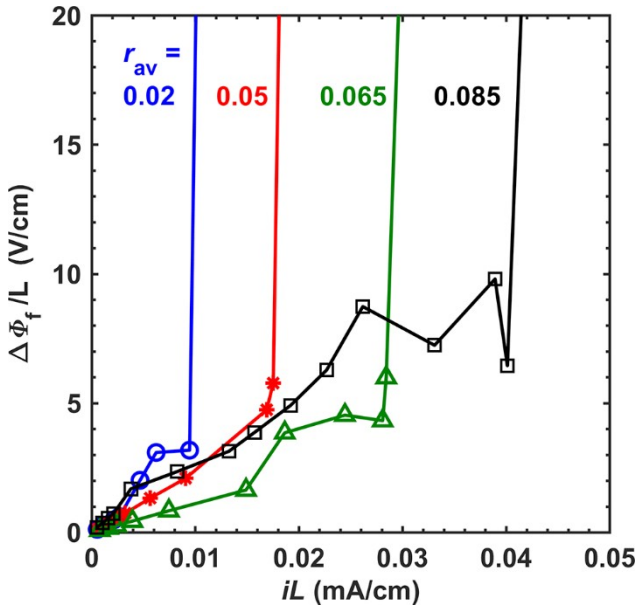

Figure 2: Length-normalized measured final cell potential, $\Delta\Phi_f$ /L, plotted against normalized applied current density, iL, for PEO/LiTFSI electrolytes in lithium symmetric cells of approximate thickness L = 250 μm at average molar salt concentrations r_{av} = 0.02, 0.05, 0.065, and 0.085. Each data point represents a unique cell, and Φ_f is the average of polarization cycles in both directions. The limiting current density, i_L, is apparent in the sharp upward inflection towards the end of each line plot.

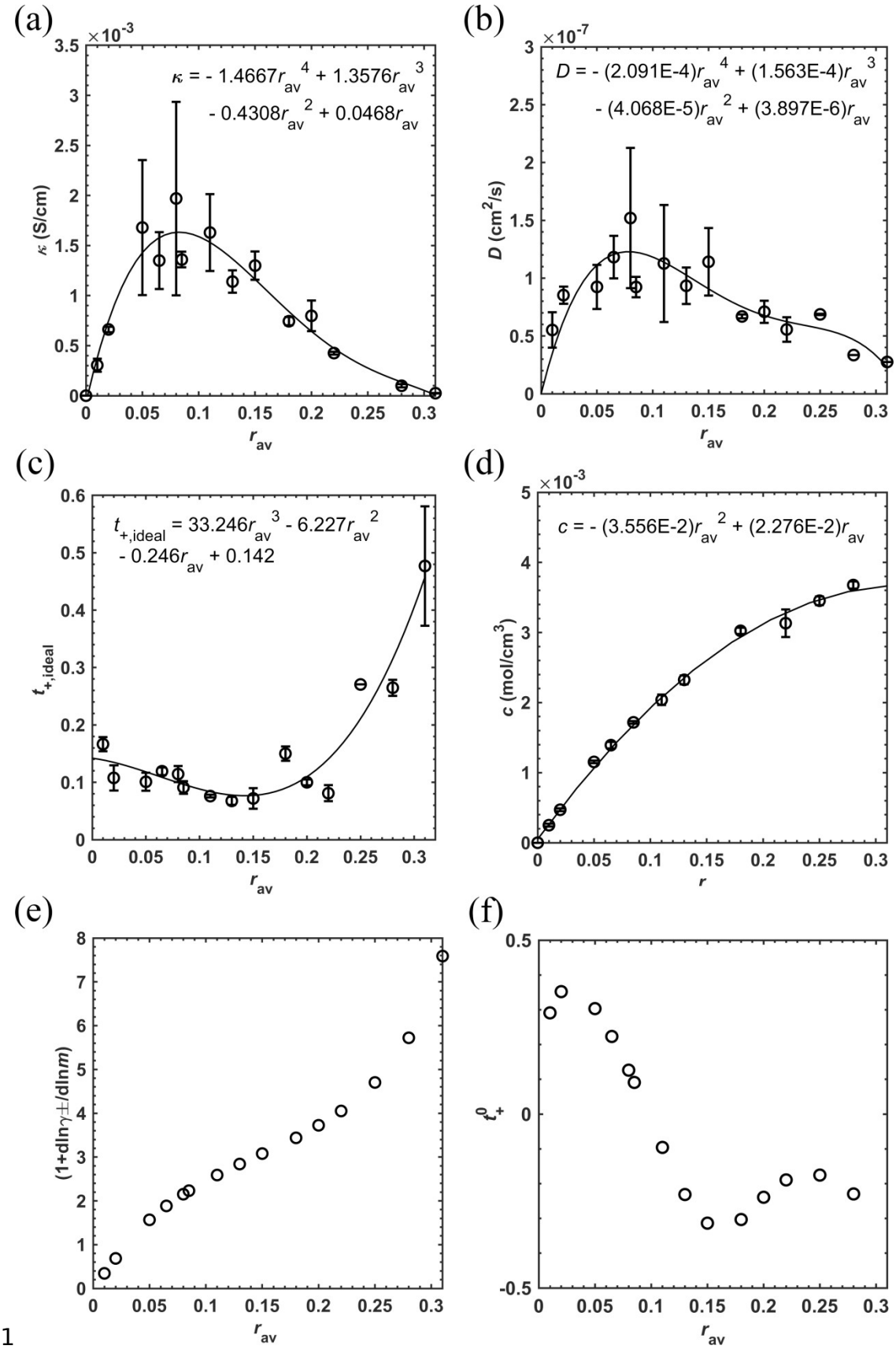
(a)
κ = - 1.4667r_{av}^4 + 1.3576r_{av}^3
- 0.4308r_{av}^2 + 0.0468r_{av}
κ (S/cm)
r_{av}
(b)
D = - (2.091E-4)r_{av}^4 + (1.563E-4)r_{av}^3
- (4.068E-5)r_{av}^2 + (3.897E-6)r_{av}
D (cm^2/s)
r_{av}
(c)
$t_{+,ideal}$ = 33.246r_{av}^3 - 6.227r_{av}^2
- 0.246r_{av} + 0.142
$t_{+,ideal}$
r_{av}
(d)
c = - (3.556E-2)r_{av}^2 + (2.276E-2)r_{av}
c (mol/cm^3)
r
(e)
(1+dln$\gamma\pm$/dln$m$)
r_{av}
(f)
t_+^0
r_{av}

521

Figure 3: (a) Ionic conductivity, κ, **(b)** diffusivity, D, **(c)** ideal transference number, $t_{+,\text{ideal}}$, **(d)** molar salt concentration, c, **(e)** thermodynamic factor $(1+d\ln\gamma_{\pm}/d\ln m)$ and **(f)** real transference number, t_{+}^{0} versus salt concentration, r_{av}, for PEO/LiTFSI electrolytes with a PEO molecular weight of 35 kg mol^{-1}, evaluated at 90 °C. Error bars represent the standard deviation of 3 trials. Fits are shown in solid black lines, and fitted values are used to evaluate **(e)** and **(f)**.

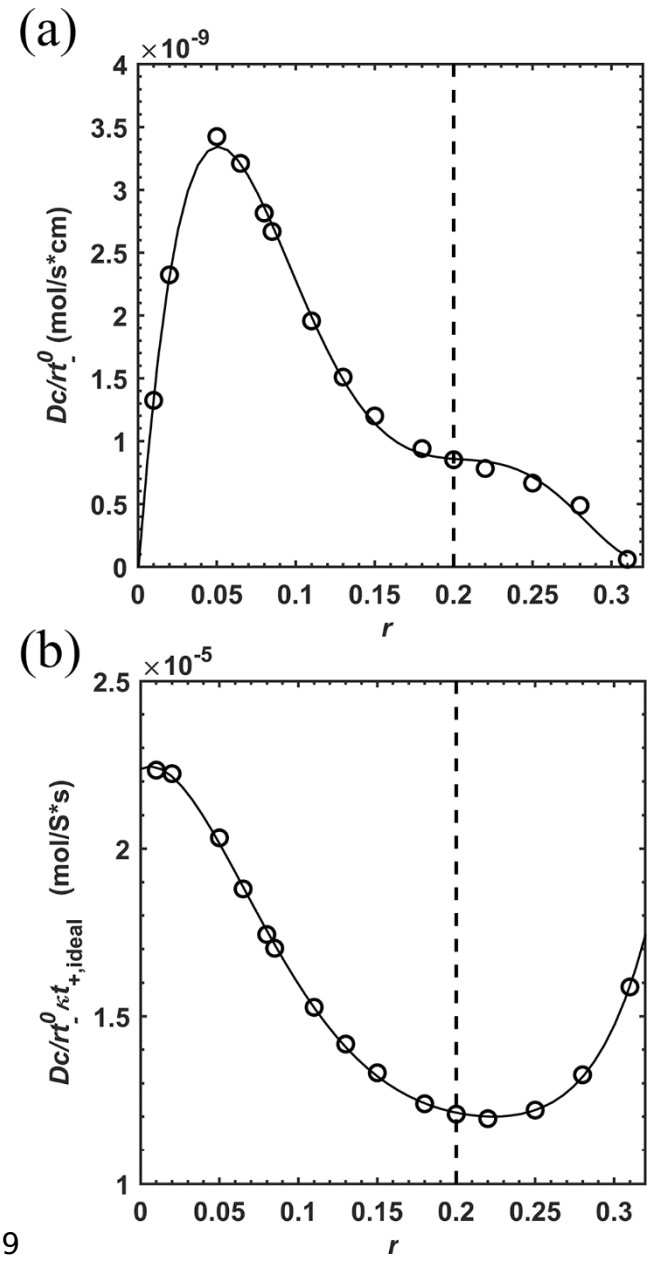

Figure 4: Polynomial fits (solid black line) to the concentration dependent transport coefficients **(a)** (Dc/rt_{-}^{0}) from Equation 3 and **(b)** $(Dc/rt_{-}^{0}\kappa t_{+,\text{ideal}})$

from Equation 4. In this study, only parameters in the range of r between 0 and 0.20 are relevant, due to the limited r_{av} values of the cells prepared.

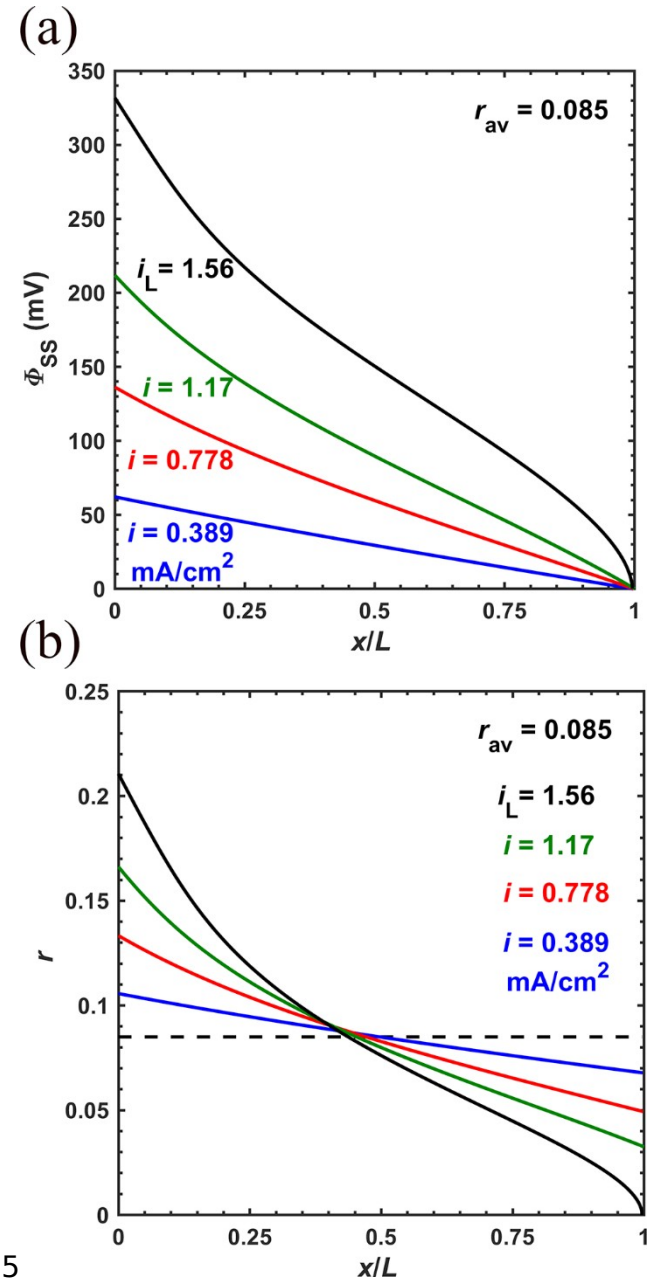

Figure 5: (a) Spatially dependent steady-state potential, Φ_{SS}, and **(b)** salt concentration, r, profiles as functions of x/L. The cell thickness L was set to 250 μm and r_{av} was 0.085. The dashed line in **(b)** represent r_{av}. The limiting current, i_L, is obtained when $r(x/L = 1)$ is zero. The chosen current densities correspond to 25%, 50%, 75%, and 100% of i_L.

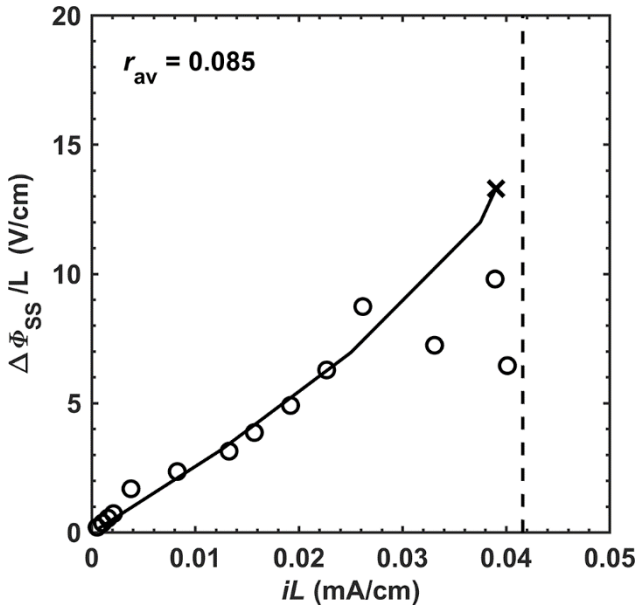

Figure 6: A comparison of experimentally measured (circles) and modeled steady-state potentials (solid line), $\Delta\Phi_{SS}/L$, versus applied current density, iL, where both axes are normalized by thickness, L. Results were obtained for PEO/LiTFSI electrolyte at 90 °C at a salt concentration r_{av} = 0.085.

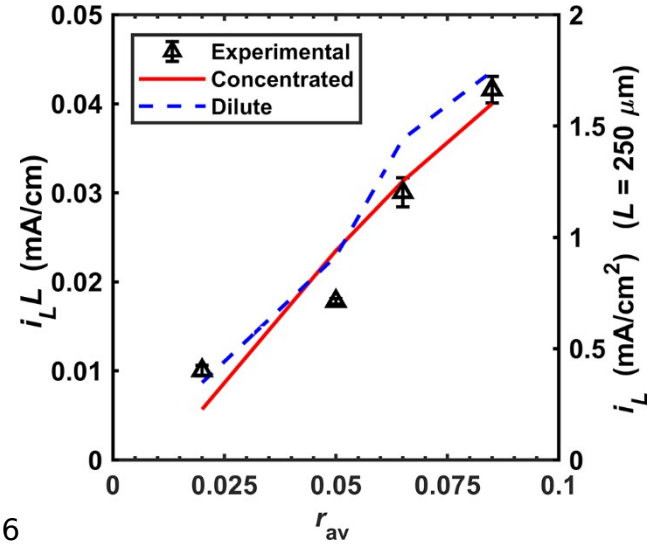

Figure 7: A comparison of predicted limiting current values from concentrated solution theory (Equations 1 and 2, red solid line), dilute solution theory (Equation 7, blue dashed line), and experimental values (triangles) plotted against salt concentration r_{av}. The left axis is normalized by electrolyte thickness L, and the right axis shows i_L values for a fixed electrolyte thickness of L = 250 μm.